Atmospheric Research 164–165 (2015) 118–130

Contents lists available at ScienceDirect

Atmospheric Research

journal homepage: www.elsevier.com/locate/atmos

New particle formation at ground level and in the vertical column over the Barcelona area

M.C. Minguillón [a,*], M. Brines [a,b], N. Pérez [a], C. Reche [a], M. Pandolfi [a], A.S. Fonseca [a], F. Amato [a], A. Alastuey [a], A. Lyasota [b], B. Codina [b], H.-K. Lee [c], H.-R. Eun [c], K.-H. Ahn [c], X. Querol [a]

[a] Institute of Environmental Assessment and Water Research, IDAEA, CSIC, Jordi Girona 18-26, 08034 Barcelona, Spain
[b] Department of Astronomy and Meteorology, Faculty of Physics, University of Barcelona, Martí i Franquès 1, 08028 Barcelona, Spain
[c] Department of Mechanical Engineering, Hanyang University, Ansan 425-791, Republic of Korea

ARTICLE INFO

Article history:
Received 26 January 2015
Received in revised form 30 April 2015
Accepted 4 May 2015
Available online 9 May 2015

Keywords:
Ultrafine aerosols
Planetary boundary layer
Nucleation
Tethered balloon
New particle formation
Vertical profile

ABSTRACT

The vertical profiles (up to 975 m a.s.l.) of ultrafine and micronic particles across the planetary boundary layer and the free troposphere over a Mediterranean urban environment were investigated. Measurements were carried out using a tethered balloon equipped with a miniaturized condensation particle counter, a miniaturized optical particle counter, a micro-aethalometer, a rotating impactor, and meteorological instrumentation. Simultaneous ground measurements were carried out at an urban and a regional background site. New particle formation episodes initiating in the urban area were observed under high insolation conditions. The precursors were emitted by the city and urban photochemically-activated nucleation occurred both at high atmospheric levels (tens to hundreds of meters) and at ground level. The new particle formation at ground level was limited by the high particulate matter concentrations recorded during the morning traffic rush hours that increase the condensation sink and prevent new particle formation, and therefore restricted to midday and early afternoon. The aloft new particle formation occurred earlier as the thermally ascending polluted air mass was diluted. The regional background was only affected from midday and early afternoon when sea and mountain breezes transported the urban air mass after particle growth. These events are different from most new particle formation events described in literature, characterized by a regionally originated nucleation, starting early in the morning in the regional background and persisting with a subsequent growth during a long period. An idealized and simplified model of the spatial and time occurrence of these two types of new particle formation episodes into, around and over the city was elaborated.

1. Introduction

The origin and processes affecting levels and variability of ambient ultrafine particles (UFP, particles smaller than 0.1 μm in diameter) in urban areas are a hot topic in both air quality and climate sciences (Charlson et al., 1992; Spracklen et al., 2010; Makkonen et al., 2012; IPCC, 2013). The main source of UFP in urban areas is road traffic (Charron and Harrison, 2003; Pey et al., 2009; Dall'Osto et al., 2013; Kumar et al., 2014; Brines et al., 2014a), and especially diesel engines (Morawska et al., 1998; Harris and Maricq, 2001; Rose et al., 2006; Rodríguez et al., 2007). Thus, studies carried out worldwide show that UFP levels are higher close to major road traffic urban arteries compared with those recorded at urban background sites (Zhu et al., 2002; Wehner et al., 2002; Kittelson et al., 2004; Hudda et al., 2010; Padró-Martínez et al., 2012; Fujitani et al., 2012). The spatial distribution of UFP across the urban environment has been studied in detail in a few cities in Europe (Dall'Osto et al., 2011, 2013; von Bismarck-Osten et al., 2013; Salma et al., 2014; Brines et al., 2014a) finding that UFP concentrations markedly increased at road sites with respect to the urban background. In addition to the prevalent primary UFP emissions governing ambient concentrations at urban sites, nucleation, agglomeration, condensation, and evaporation processes have an effect on UFP concentrations and size (Charron and Harrison, 2003; Kulmala et al., 2004; Robinson et al., 2007; Dall'Osto et al., 2011; Harrison et al., 2012).

A number of studies in the beginning of the last decade first pointed to the occurrence of new particle formation episodes in urban environments (Woo et al., 2001; Alam et al., 2003; Stanier et al., 2004). Subsequent studies evidenced the relevance of these episodes in cities from high insolation regions such as southern Europe, California or Australia (Pey et al., 2008; Costabile et al., 2010; Reche et al., 2011; Hudda et al., 2010; Cheung et al., 2011, 2015; Brines et al., 2014b). This influence is so important that, on an annual average, maximum hourly UFP concentrations at the urban background of Barcelona (Northeast of Spain) are recorded at midday simultaneously with the lowest black carbon (BC) concentrations (Reche et al., 2011). The new

* Corresponding author. Tel.: +34 934006100.
E-mail address: mariacruz.minguillon@idaea.csic.es (M.C. Minguillón).

http://dx.doi.org/10.1016/j.atmosres.2015.05.003

particle formation events studied in the cities of Barcelona, Brisbane, Los Angeles, Madrid, and Rome by Brines et al. (2014b) showed nucleation bursts without important subsequent particle growth, different from the typical 'banana-like' nucleation episodes usually described in regional background environments (Kulmala et al., 2004; Kulmala and Kerminen, 2008). The lack of a relevant growing stage was attributed to the delay in the start of the new particle formation in urban environments with respect to the regional background, where new particle formation starts in the morning. This delay is due to the increase of the condensation sink (CS) during the morning and afternoon road traffic rush hours. Thus new particle formation takes place in the city only when primary pollutant concentrations are low, i.e. after the concentration of traffic primary pollutants has decreased at midday, and until the afternoon rush hour.

Two major types of new particle formation episodes in the urban area of Barcelona were identified by using four simultaneous Scanning Mobility Particle Sizer (SMPS) instruments into the city and in the regional background during the SAPUSS campaign (Dall'Osto et al., 2013). One occurs on a regional scale and hence it is simultaneously recorded at the regional background and urban sites, with the differences in growth and time extension described above. The other type starts in the city and affects the regional background in a delayed stage by the transport of the nuclei and/or the precursors. The time delay is attributed to the availability of chemical precursors in the city (Dall'Osto et al., 2013). These midday urban new particle formation episodes are favoured by the high insolation and the decrease of the CS caused by the dilution of pollutants due to reduced emissions, growth of the planetary boundary layer (PBL) and maximum sea breeze flow intensity. Furthermore, the sea breeze transports SO_2 from shipping emissions that may help to activate nucleation. Similarly to these urban new particle formation episodes, Setyan et al. (2014) reported that the occurrence of new particle formation events in the regional background of Sierra Nevada (US) was associated with the influence of the urban plumes of Sacramento.

Studies carried out in London at different heights suggested that during the upwards convective transport of urban air pollutants as the PBL grows, important volatilization processes occur affecting the external shells of semi-volatile organic matter of UFP (Dall'Osto et al., 2011; Harrison et al., 2012). These volatilized organic substances are very reactive and they may yield to the formation of a large amount of newly formed particulate matter (Robinson et al., 2007). In any case, studies on the urban vertical distribution of UFP are very scarce, especially those covering the whole PBL, given that special instrumentation is required to measure UFP concentrations using balloons, or other airborne settings, throughout the vertical profile of the PBL (Ahn and Eun, 2013). Wehner et al. (2007) designed a study with four ground sites in Leipzig, Germany, separated up to 50 km, and a tethered balloon equipped with a combination of two Condensation Particle Counters (CPC) with different lower size detection limits so that the particle number concentration between 5 and 10 nm was deduced. They found two different nucleation scenarios, namely (i) homogeneous case, during which new particle formation was measured at the different ground sites nearly in parallel with subsequent particle growth and the UFP were found to be well mixed within the entire PBL; and (ii) inhomogeneous case, during which new particle formation was observed at one to three ground sites irregularly and subsequent particle growth was often interrupted. In this latter case, the new particle formation was found to depend mainly on the incoming solar radiation, but other factors must account for the inhomogeneous occurrence of the event in the study area. Some other studies on the vertical distribution of aerosols with in-height and/or tethered balloon borne instrumentation exist but they do not include the UFP size range (e.g. Matsuki et al., 2005; Greenberg et al., 2009; Ferrero et al., 2010, 2011; Babu et al., 2011; Moroni et al., 2012, 2013; Hara et al., 2013, 2014) and therefore the new particle formation processes could not be investigated.

The vertical profiles of aerosol properties have been determined using different instrumentation. Thus, Ma and Yu (2014) measured the aerosol extinction up to 5 km and found that it is mainly located below 1 km, with larger percentages in winter seasons (62–79%) and smaller percentages in summer seasons (44–57%), and attribute these differences to the strength of vertical transport. Moreover, they link the aerosol extinction to secondary particles whereas that attributed to other aerosol species is relatively small and only limited near the surface. Fernández-Gálvez et al. (2013) combined ground and column measurements, finding that anthropogenic aerosol in the atmosphere in the absence of a well-developed mixing layer is not exponentially distributed with height, and concluded that estimates of columnar aerosol optical and microphysical properties from ground measurements are not straightforward.

The main objective of this study is to analyze how the new particle formation takes place over an urban Mediterranean environment, by investigating the vertical distribution of UFP throughout the PBL height (PBLH) and the free troposphere. To this end measurements were carried out using a tethered balloon equipped with miniaturized CPC and optical particle counters (OPC) (Lee et al., 2014), a microaethalometer, a rotating impactor, instrumentation to measure meteorological variables (wind speed and direction, temperature and relative humidity) and a GPS. Vertical profiles up to 975 m a.s.l. were studied from 13 to 15 May 2014 between 8:00 and 16:00 local time with different sampling strategies regarding the ascending and descending velocity and the time spent at maximum height. To support interpretations, simultaneous measurements of aerosol parameters (concentration, size and composition), gaseous pollutants ambient concentrations, and meteorological parameters were carried out at two ground monitoring stations (one urban and one regional background).

2. Methodology

2.1. Measurement area, sites, and schedule

The measurements were carried out in the Northeast of Spain, in the Western Mediterranean Basin (WMB). This area is characterized by mild winters, warm summers and prevalent clear sky conditions all year round. Solar radiation is thus intense, its maximum values ranging from 450 to 900 W/m^2 at midday. Precipitations are scarce and usually concentrated in spring and autumn. More characteristics of the WMB can be found in Millán et al. (2000). The city of Barcelona is geographically constrained by the coastal range of Collserola to the North and the Mediterranean Sea to the Southeast, thus being influenced by the sea-breeze dynamics. This results in a dominant Northwest wind component during the night and the development of sea breezes during the day. The diurnal breezes turn progressively from Southeast to Southwest and the gradually increasing wind speed reaches its maximum levels around noon when the boundary layer is fully developed (Pérez et al., 2004). Moreover, different meteorological scenarios can have an impact on the air pollution of the city, ranging from stagnant anticyclonic conditions, recirculation of air masses or Atlantic air mass advection to African dust outbreaks. The main source of atmospheric pollution in Barcelona is road traffic (e.g. Amato et al., 2009; Pérez et al., 2010; Reche et al., 2011), although emissions from industry, power generation, construction, domestic and residential sectors, and harbor activities are also relevant.

The balloon measurements location was situated in the city of Barcelona, in an open area from the Real Club de Polo de Barcelona. The balloon flights were carried out during 13 to 15 May 2014 according to the schedule in Table 1. Local time in Barcelona is GMT + 2. All reported times in this study correspond to local time. One flight up to 800 m a.s.l. from 8:29 to 10:34 was carried out on the 13 May. Two flights were performed on the 14 May, from 8:12 to 10:35 (up to 800 m a.s.l.) and from 12:01 to 15:52 (up to 975 m a.s.l.). On 15 May the measurements were carried out during an ascending flight from 8:00 to 9:30 up to 900 m a.s.l. and a short descending flight down to 770 m a.s.l. (until 10:28). Subsequently the measurements were carried out at a constant height (about 700 m a.s.l.) until 16:00.

Table 1
Schedule of balloon flights, with indication of the impactor samples taken.

Date	Start time	End time	Balloon direction	Impactor samples	Observations
13 May 2014	8:29	9:22	Ascending		
	9:23	10:34	Descending		Non-valid Hy-CPC data
					No more flights due to rain
14 May 2014	8:12	9:23	Ascending	9:19–9:49 #6	
	9:25	10:35	Descending		
	12:01	13:38	Ascending	13:05–13:35 #7	
	13:40	15:52	Descending	13:43–13:58 #8	Non-valid Hy-CPC data from
				14:01–14:16 #9	13:40 to 13:57 (about 700 m.a.s.l.)
				14:20–14:35 #10	13:57 pump re-start
				15:06–15:21 #11	
				15:27–15:37 #12	
				15:47–16:02 #13	
15 May 2014	7:00	8:00	Ground	7:06–7:36 #14	7:47 Hy-CPC flow rate calibration
	8:00	9:30	Ascending	8:09–8:36 #15	8:16 pump re-start
				9:04–9:34 #16	
	9:31	10:28	Descending	9:35–10:39 #17	9:57 Hy-CPC pump re-start Stop descending at around 770 m a.s.l.
	10:30	16:02	Stable	10:25–10:55 #18	10:01 Hy-CPC pump re-start
				11:09–11:39 #19	
				12:41–13:11 #20	

Simultaneous measurements were carried out at two ground sites. The urban background site Palau Reial was about 500 m far from the balloon location (41°23′14″ N, 02°06′56″E, 78 m a.s.l.). It is influenced by vehicular emissions from one of the main traffic avenues of the city, located at a distance of 200 m (traffic density of 11,8000 vehicles/day; Ajuntament de Barcelona, 2014, http://w110.bcn.cat/Mobilitat/Continguts/DADESBASIQUES2013_p2.pdf). The regional background site of Montseny (41°46′46″N, 02°21′29″E, 720 m a.s.l.) was located in a natural park 40 km to the NNE of Barcelona and 25 km from the coast. This site represents the regional background of the NE Iberian Peninsula (Pérez et al., 2008; Pey et al., 2008; Seco et al., 2011) and is a member of the ACTRIS (Aerosols, Clouds, and Trace gases Research InfraStructure) and GAW (Global Atmosphere Watch) networks (Fig. 1).

2.2. PBLH determination

Radiosounding data is available from the Catalan Meteorological Office. Free balloons are launched daily in Barcelona from the Faculty of Physics, located at 300 m from the Palau Reial site (Fig. 1). The PBLH at 14:00 and 02:00 was calculated using the simple parcel method described by Holzworth (1967). The parcel method allows the determination of the PBLH in the case of marked inversions, which are usually observed at midday but are also typical for the nocturnal atmosphere (e.g. Pandolfi et al., 2014). With this method the PBLH is taken as the equilibrium level of an air parcel with the potential temperature (T_{pot}) calculated at ground level. The water vapor mixing ratio (χ) was calculated with the humidity conversion formulas provided by Vaisala

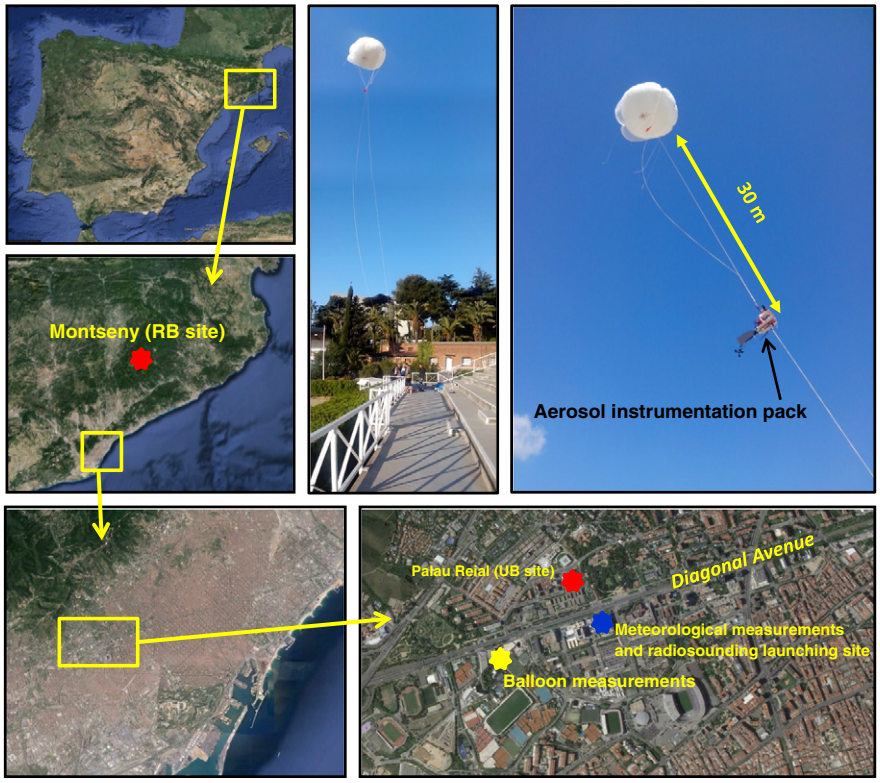

Fig. 1. Location of the ground and balloon measurement sites and pictures of balloon and equipment.

(2013). Given that the launching site of the weather balloons was at 98 m a.s.l., the calculated PBLH may be underestimated. The vertical profiles of T_{pot} and χ at 14:00 and 02:00 were used together with the vertical profiles of T_{pot} and χ from the tethered balloon to study the thermodynamic state of the lower atmosphere. The apparent discrepancy between the different vertical profiles (from radiosounding measurements and from the tethered balloon measurements) can be explained by the fact that radiosounding measurements use free balloons which reach the top of the PBL typically in few minutes, as opposed to the tethered balloon, which can take up to 1.5 h to reach 1000 m. Moreover, the times of the different profiles were not the same.

2.3. Air mass origin

The air mass origin was determined based on air back trajectories calculated using the HYSPLIT (Hybrid Single Particle Lagrangian Integrated Trajectory Model) model from the NOAA Air Resources Laboratory (ARL) (Draxler and Rolph, 2003). Five-day back trajectories were calculated on each of the study days at 6, 9, 12 and 15 h GMT modeling vertical velocity and for 3 different heights (750, 1500 and 2500 m a.g.l.).

2.4. Balloon characteristics and instrumentation

A tethered balloon of 27 m^3 filled with He was used. An aerosol instrumentation pack was attached 30 m below the balloon. The instruments included in the pack were as follows (Fig. 2):

- A miniaturized condensation particle counter (Hy-CPC), which measured particle number concentration larger than 3 nm with a time resolution of 1 s and a flow rate of 0.125 L/min, using isopropyl alcohol as the working fluid (Lee et al.,2014). The particle number concentration measured by the Hy-CPC will be referred to as $N_{>3}$. Note that it should be interpreted as UFP, given that around 70–90% of the total particle number concentration is made by UFP (Charron and Harrison, 2003).
- A miniaturized optical particle counter (Hy-OPC), which measured particle number concentrations in the ranges of 0.3–0.5 μm, 0.5–1.0 μm, 1.0–2.0 μm and 2.0–5.0 μm, with a time resolution of 1 s and a flow rate of 1 L/min (Lee et al.,2014).
- A rotating impactor, which collected microscope samples in three size stages (1–2.5 μm, 2.5–10 μm, and >10 μm), with a flow rate of 1 L/min.
- A microaethalometer (MicroAeth AE51), which measured BC concentrations derived from absorption values on a 5 min basis with a flow rate of 0.15 L/min. Valid data only on 15 May 2014.
- A Global Position System (GPS).
- An accelerometer.
- Temperature, relative humidity, pressure, wind direction and speed sensors.
- A control board to communicate with a computer located on the ground so that all the measurements could be tracked in real time.

Monitoring sensors are usually attached to fixed supports. In this case, however, they were suspended from a tethered balloon, which could be a matter of concern under erratic or turbulent motions that could affect sensor measurements. These motions were assessed using the GPS and accelerometer data, showing that balloon accelerations were of the same order as wind accelerations thus indicating that the aerostat smoothly adapted its position to the blowing wind with no sharp movements. Visual observations revealed the same. Therefore the lack of a fixed support for the aerosol pack is not expected to have had any influence on the measurements.

Fig. S1 shows the comparison of ambient particle number concentration measured with collocated Hy-CPC and a CPC TSI 3776, both with a similar size detection limit of around 3 nm. Results evidenced very comparable concentrations, with r^2 between 0.65 and 0.98, and slopes between 0.87 and 1.23. The concentrations reported in the present study corresponding to the vertical profiles have been calculated to be in normal conditions (25 °C, 1013.2 hPa).

2.5. Ground site instrumentation

2.5.1. Urban background site

Particle number size distributions within the range of 10–480 nm (N_{10-480}) were measured with a SMPS, composed by a Differential Mobility Analyser (DMA, TSI 3081) coupled with a CPC (TSI 3772). Equivalent BC mass concentrations (Petzold et al., 2013) were measured by a multi-angle absorption photometer (MAAP, model 5012, Thermo ESM Andersen Instruments) with a PM_{10} inlet. On-line PM_{10}, $PM_{2.5}$, and PM_1 concentrations were measured by an OPC (GRIMM 180) and corrected with simultaneous 24-hour gravimetric samples. An Aerosol Chemical Speciation Monitor (Aerodyne Research Inc., ACSM; Ng et al., 2011) was used to measure real time non-refractory submicron aerosol species (organic matter, nitrate, sulfate, ammonium and chloride). Real time monitors for NO, NO_2 (SIR S-5012), O_3 (SIR S-5014), and SO_2 (Thermo Scientific Model 43C) were supplied by the Department of Environment of the Autonomous Government of Catalonia. Atmospheric pressure, wind components, solar radiation, temperature and relative humidity were recorded by the Faculty of Physics from the University of Barcelona in a meteorological station located at a height of 108 m a.s.l. at 300 m from the urban background site (Fig. 1).

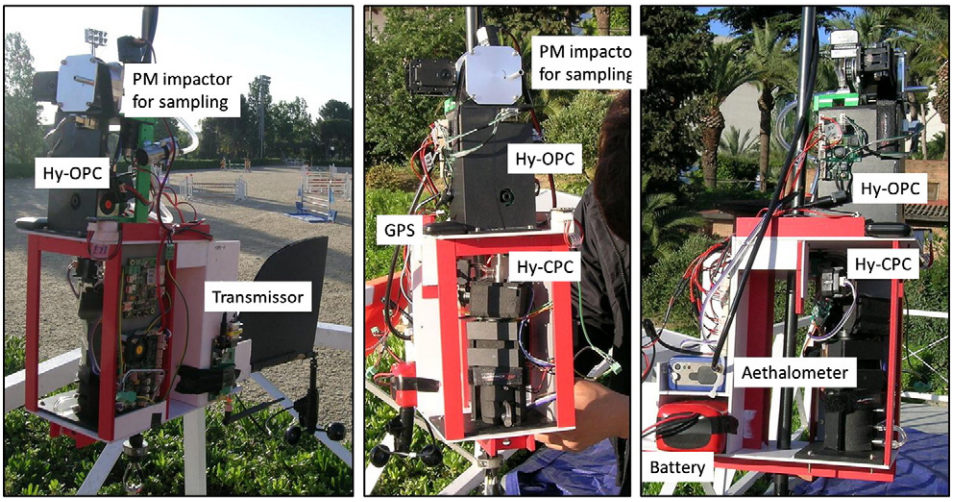

Fig. 2. Details of the instrumentation included in the aerosol pack for balloon measurements.

2.5.2. Regional background site

Particle number size distributions within the range of 9–860 nm were measured using a SMPS, comprising a DMA connected to a CPC (TSI 3772). This system was designed and manufactured in the framework of the EUSAAR project at the Leibniz Institute for Tropospheric Research (TROPOS; Wiedensohler et al., 2012). Total particle number concentrations in the size range between 3 and 1000 nm ($N_{>3}$) were measured with an ultrafine CPC (UCPC, TSI 3776). On-line BC, PM_{10}, $PM_{2.5}$, and PM_1 concentrations were measured using similar instrumentation as that used in the urban background site. Real time monitors for O_3 (MCV, 48 AUV), NO, NO_2 (Thermo Scientific Model 42i-TL, trace level), and SO_2 (Teledyne instruments Model 100E) were supplied by the Department of the Environment of the Autonomous Government of Catalonia. Wind direction, wind speed, solar radiation, temperature, relative humidity and precipitation were also recorded.

2.6. TEM and SEM analysis

Using the rotating impactor, particles for transmission electron microscopy (TEM) or scanning electron microscopy (SEM) observation were collected onto Quantifoil® gold (Au) grids with 1 μm diameter holes–4 μm separation of 200-mesh. Gold grids were mounted covering the whole impacting area for each of the size-fractionated particles stages (1–2.5 μm, 2.5–10 μm, and >10 μm). The impactor had 24 sampling positions for each of the size stages and was remotely operated from the ground in such a way that 30 min samples were collected at different heights and times on single sample holders (Table 1).

Particle morphology, chemical composition, and size were analyzed in Spain by TEM (Jeol, JEM 1220, Japan) or SEM (FEI, Quanta 200 FEG, USA), both coupled with an energy-dispersive X-ray (EDX) spectroscopy; and in Korea by a SEM (Jeol, JSM-6390, USA) equipped with an Oxford Link SATW ultrathin window EDX detector.

In order to identify the particle composition at different altitudes, more than 100 particles per $PM_{1-2.5}$ sample collected on 14 May 2014 at the free troposphere (sample #6), top of the PBL (sample #7), middle of the PBL (sample #10), and at ground level (sample #13), and more than 100 particles per $PM_{1-2.5} + PM_{2.5-10}$ samples collected on 15 May 2014 at the top of the PBL (sample #19), the free troposphere (sample #16), and at ground level (sample #14) were semi-quantified by SEM-EDX microanalysis. The abundance of mineral matter (SiO_2, Fe_2O_3, Al_2O_3, K_2O and CaO), sea salt (Mg + Na + Cl) and sulfate was assessed.

3. Results

3.1. Meteorological conditions

The sampling period included from 13 to 15 May 2014. Light rain took place on 12 May, leading to a clean atmosphere at the start of the measurements. The 13 May was cloudy with sporadic very light rain and solar radiation intensity below 60 W/m^2 at noon. Mild temperatures from 13 to 15 °C and 68 to 81% RH were registered at ground level.

On 14 and 15 May 2014, clear, dry, and warm conditions prevailed. The temperature ranged from 19 to 27 °C and 17 to 25 °C on the 14 and 15 May, respectively. The RH ranged from 31 to 47% and 37 to 64% on the 14 and 15 May, respectively. The sea breeze was developed on both the 14 and 15 May, from 12:00 to 22:00, with prevailing S–SW wind direction and wind speed of 1–2 m/s on the 14 May and 2 m/s on the 15 May.

3.2. 13 May 2014 measurements

This was a cloudy day with very mild advective circulation and mild temperatures, from 13 to 15 °C and 68 to 81% RH at ground level, and from 8.5 to 8.8 °C and 91 to 92% RH at 800 m a.s.l. during the balloon measurements. Very light rain occurred during the descending flight. The analysis of air mass back trajectories indicates that air masses originated dominantly from the West (about 2500–3000 km far) (Fig. S2). The solar radiation intensity was lower than 60 W/m^2 at noon, which prevented the development of the boundary layer. The PBLH at 14:00 was around 750 m a.s.l., whereas a lower PBLH was detected at 02:00 (550 m a.s.l.) (Fig. 3). The vertical profiles of χ confirmed that the highest concentrations of liquid water were observed in these altitude ranges. During the flight with the tethered balloon (8:29–10:34), ascending up to 800 m a.s.l., the PBLH was at around 400–600 m a.s.l.

These conditions yielded an early morning (08:29–09:22) vertical profile of $N_{>3}$ characterized by an upward decreasing gradient (from 28,500 to 10,000 #/cm^3) up to around 500 m a.s.l., and from there another upward increasing trend (up to 34,000 #/cm^3) up to 800 m a.s.l. (Figs. 4 and S2). At ground level, maximum N_{10-480} during the morning rush hour peak was 19,500 #/cm^3 (Fig. 5), mainly due to an increase of the 50–100 nm fraction, with a simultaneous increase in BC, NO_2 and SO_2 concentrations (Fig. 5).

Number concentrations of 0.3–0.5, 0.5–1.0 and 1.0–5.0 μm particles in the vertical profile were also relatively constant with a slight upwards increasing trend from 22 to 50 #/cm^3 in the 0.3–0.5 μm fraction from ground to 700 m a.s.l., and an abrupt increase from 700 to 760 m a.s.l. due to the influence of clouds (RH around 100%) (Fig. 4). Temperature gradient was characterized by an adiabatic trend from 15 to 8 °C, whereas RH, as expected, exhibited an inverse trend from 70 to 90% at about 700 m a.s.l., and reached 100% at 800 m a.s.l. A similar vertical profile was evidenced during the descending measurements (09:23–10:34) for T, RH and particles >0.3 μm, the latter with some increases attributed to clouds. The $N_{>3}$ measurements during the descending flight were invalidated due to the massive condensation of water on the instrument.

At the Montseny regional background site maximum N_{3-10} concentrations reached only 4000 #/cm^3 and only for a short period (about 1 h) after midday (Fig. 5), probably due to the development of mountain breeze flows that transported UFP from the urban to the mountain areas.

3.3. 14 May 2014 measurements

This was a clear, dry, and warm day, with 19 to 27 °C and 31 to 47% RH at ground level, and from 14 to 15 °C and 47 to 51% RH at 900 m a.s.l. during the balloon measurements. The 5-day back trajectory at 750 m a.g.l. indicates that the dominant air mass origin was from the Northwest (at about 3500 km) (Fig. S2). The wind direction during the first ascending flight turned from the NW at heights between 0 and 400 m a.s.l. to NW–SW between 400 and 600 m a.s.l., and it changed to SW from 600 to 800 m a.s.l. During the entire first descending flight the wind direction was SW (Fig. S3). During the second ascending flight (starting at 10:21), the sea-breeze was already developed, and the wind direction was mainly from the S–SW between 0 and 800 m a.s.l., and switched to SW–W between 800 and 1000 m a.s.l. During the descending flight the wind direction stayed at SW–W between 1000 and 800 m a.s.l. and it was S–SW during the rest of descending flight to the ground. The PBLH at 02:00 and 14:00 was around 650 and 1110 m a.s.l., respectively (Fig. 3). The lower PBLH during the night is a consequence of the reduction of convective activity driven by the heating of the Earth's surface and the corresponding nocturnal radiative cooling of the ground. During the first balloon ascending flight the PBLH was around 500 m a.s.l. and it was around 600 m a.s.l. during the descending flight. This is in agreement with the change in wind direction observed during the ascending flight at around 600 m a.s.l (Fig. S3). Higher PBLH was measured during the second flight in the afternoon, reaching altitudes higher than 800–1000 m a.s.l. (maximum altitudes reached by the tethered balloon).

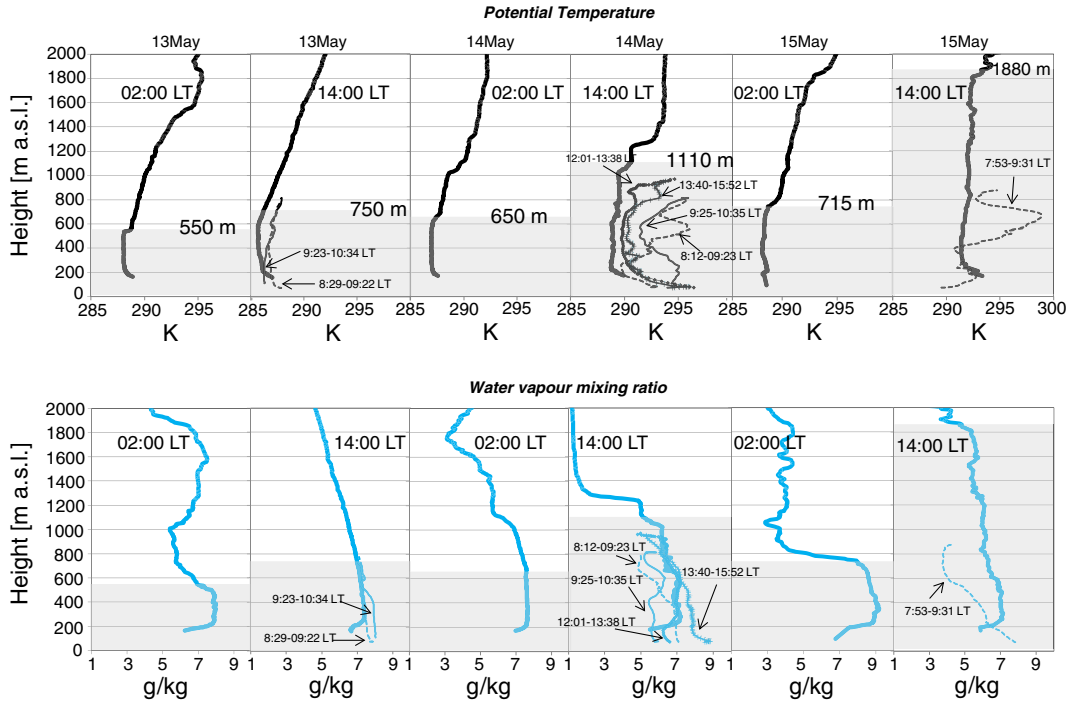

Fig. 3. Vertical profiles of potential temperature (T_{pot}, up) and water vapor mixing ratio (χ, bottom) at 02:00 and 14:00 from radiosoundings in Barcelona during the period 13–15 May 2014. Also shown are the vertical profiles of T_{pot} and χ from the tethered balloon at different times. Shaded in grey the calculated planetary boundary layer height.

3.3.1. First flight

Early in the morning (8:12–9:23) $N_{>3}$ and 0.3–0.5 μm particles concentrations showed an increasing trend from ground up to around 200 m a.s.l. where the highest concentrations were reached ($N_{>3}$ and 0.3–0.5 μm particles concentration increased from 25,000 to 95,000 and from 55 to 70 #/cm^3, respectively). In this lower layer the T_{pot} strongly decreased with height indicating a quite unstable atmosphere likely allowing the transport of pollutants from ground upwards. From 200 m a.s.l. to around 600 m a.s.l. the $N_{>3}$ decreased to 7000 #/cm^3, remaining then relatively constant up to 800 m a.s.l. (8000–5000 #/cm^3) (Figs. 4 and S4). Hence these latter lower concentrations probably represent the cleaner free troposphere, in agreement with the PBLH. In addition to the gradients described, narrow (10 m thick) strata with very different $N_{>3}$ were identified (Fig. S4). The 0.3–0.5 μm particle concentration decreased to 25 #/cm^3 from 200 m a.s.l. to 600 m a.s.l., and increased up to 40 #/cm^3 at 820 m a.s.l. A similar trend was followed by the 0.5–1.0 and 1.0–5.0 μm particles (Fig. 4).

Simultaneously, at ground level (Fig. 5), particle size distributions and BC concentrations reflected the traffic rush hour (maximum N_{10-480} 19,300 #/cm^3 and 3.2 μg/m^3 of BC), followed by a significant decrease (down to 5000 #/cm^3 and 0.5 μg/m^3) due to the development of the boundary layer. Organic matter, nitrate, ammonium and sulfate concentrations increased at 6:00 and remained relatively high until 9:00 (with average concentrations higher than the previous day) (Fig. 6). A similar trend was observed for the road traffic organic tracer at *m/z* 55 (Canagaratna et al., 2004) as well as for the secondary organic aerosol tracers (*m/z* 43 and *m/z* 44) (Zhang et al., 2005) from the organic mass spectra registered by the ACSM. The ratio of the *m/z* xx signal to the total organic signal in the ACSM mass spectra is shown in Fig. 6 as fxx.

During the descending flight (9:25–10:35, after the traffic rush hour peak) the concentration of all particulate size fractions was diluted by a factor of at least 2 with respect to the ascending trajectory (Figs. 4 and S4). Thus, at altitudes from 815 to 520 m a.s.l. $N_{>3}$ reached 1500–2000 #/cm^3, and from there to the ground a slight and progressive increase up to 30,000 #/cm^3 was measured, with stratification being less marked than in the ascending profile. For the 0.3–0.5, 0.5–1.0 and 1.0–5.0 μm fractions, there was also a dilution factor of 2 with respect to the ascending trajectory, but the maximum recorded at 200 m a.s.l. was shifted to 650 m a.s.l. coinciding with the T_{pot} inversion with the stable atmosphere above.

3.3.2. Second flight

The vertical profiles during the second ascending flight of the day (12:01 to 13:38) can be segmented in four parts. The first part includes from ground up to 400 m a.s.l., which is the lower layer characterized by quite unstable atmospheric conditions with T_{pot} decreasing with height (Fig. 3). The vertical profile was characterized by a marked increase of $N_{>3}$ from around 35,000 to 50,000 #/cm^3 and a simultaneous increase of coarser particles, with concentrations from 33 to 113 #/cm^3 for 0.3–0.5 μm particles (Figs. 4 and S4). Less stratification than in the morning flight was observed probably due to better homogenization of the PBL by the intensive convective dynamics (Fig. S4). From 420 to 525 m a.s.l., an increase in $N_{>3}$ and a simultaneous decrease in coarser particles were recorded. From 525 to 930 m a.s.l., a layer with almost constant T_{pot} with height, where the inversion was detected, the $N_{>3}$ increased (reaching around 62,000 #/cm^3) and the 0.3–0.5, 0.5–1.0 and 1.0–5.0 μm concentrations followed a clearly opposite trend, slightly decreasing from 113 to 80 #/cm^3 for the 0.3–0.5 μm particles. Finally, the last segment covers from 930 to 975 m a.s.l., where the $N_{>3}$ decreased down to 21,000 #/cm^3.

The high $N_{>3}$ and micronic particulate concentrations registered from ground to 975 m a.s.l. are typical from the PBL and not from the free troposphere, which is in agreement with the PBLH of 1100 m a.s.l. determined by radiosoundings at 14:00 (Fig. 3). These high $N_{>3}$ concentrations recorded at different heights can be attributed to new particle formation events induced by the low RH and high temperature and insolation and the dispersion of pollutants.

Simultaneously, a new particle formation event took place at ground level. An increase in N_{15-30} attributed to photochemical nucleation processes starting at 11:00 was detected, with a growth until 14:30 (Fig. 5). An increase in BC (up to 2.4 μg/m^3, Fig. 5), organic aerosols, nitrate, ammonium and sulfate concentrations (Fig. 6) was also recorded. The formation of secondary organic aerosol is supported by the variations in the different organic tracers. Whereas the marker for road traffic

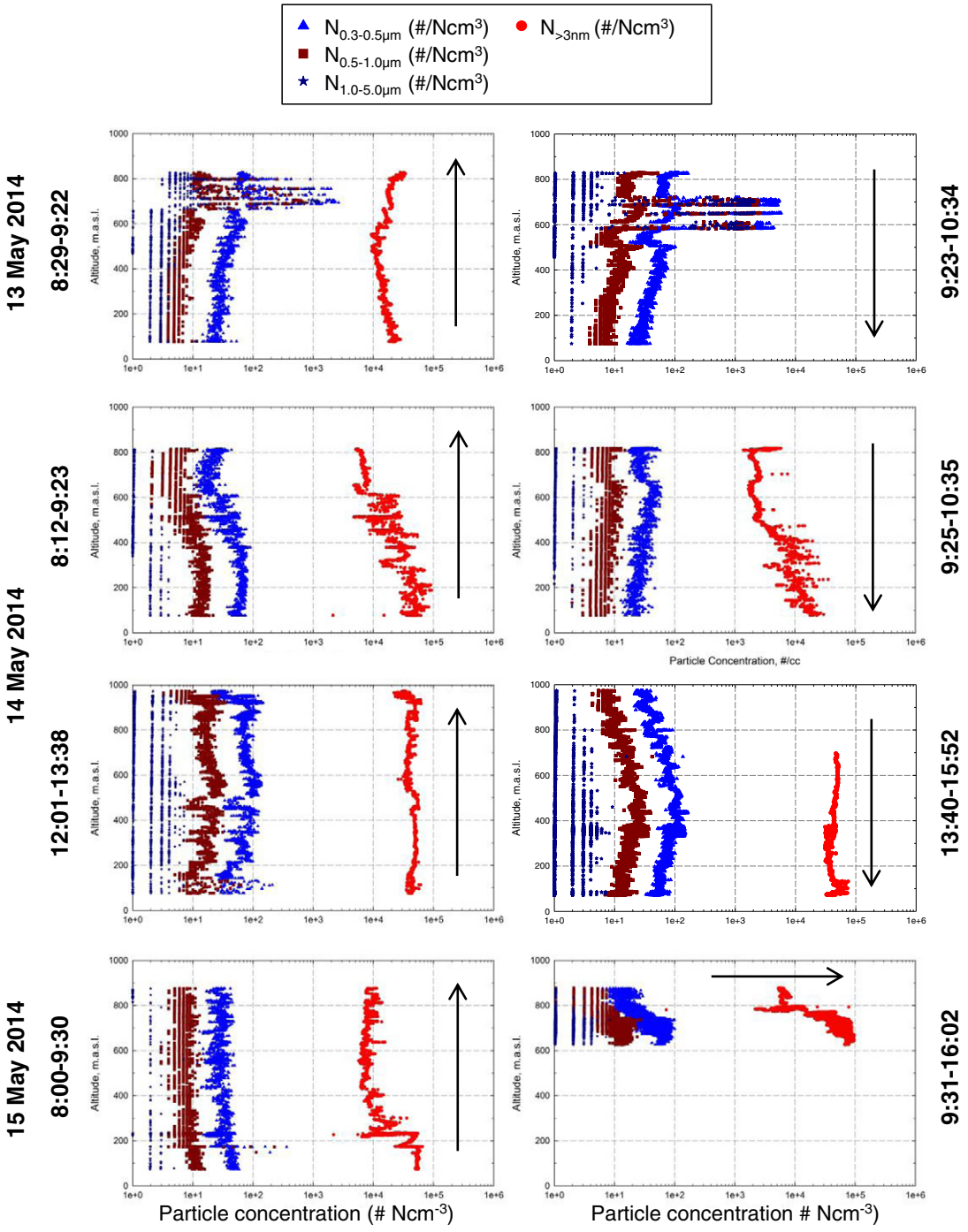

Fig. 4. Vertical profiles of $N_{>3}$ (# Ncm^{-3}) (Hy-CPC), 0.3–05 μm, 0.5–1.0 μm, 1.0–5.0 μm, 5.0–10.0 μm (Hy-OPC). Arrows indicate the sense of the balloon profile (ascending, descending or kept at a given height).

primary organic aerosol (*m/z* 55) experimented a moderate increase, those for secondary organic aerosol (*m/z* 43 and *m/z* 44) increased in a higher proportion. A change in the wind direction at 12:30 resulted in a sharp reduction of N_{10-480} for 15 min, as particles were advected away by a change of air parcel. This change coincides with an increase in wind speed, BC, NO_2 and SO_2 concentrations (Fig. 5). SO_2 concentrations reached a maximum of 4 μg/m^3, which could explain the increase in sulfate concentrations (reaching about 1.5 μg/m^3, Fig. 6).

The descending measurements (13:40 to 15:52) can be divided in three segments (Figs. 4 and S4). From 970 to about 350 m a.s.l. the $N_{>3}$ decreased from around 52,000 to 37,500 #/cm^3 (note that the Hy-CPC data from 970 to 700 m a.s.l. was discarded due to anomalous measurements), whereas the 0.3–0.5, 0.5–1.0 and 1.0–5.0 μm particle concentrations increased. The second segment includes from 350 to about 140 m a.s.l. During this segment, a reverse trend was recorded for both $N_{>3}$ (increasing to 46,000 #/cm^3) and 0.3–0.5, 0.5–1.0 and 1.0–5.0 μm particles (decreasing). Finally, whereas the 0.3–0.5, 0.5–1.0 and 1.0–5.0 μm particles continued decreasing down to the ground, the $N_{>3}$ showed an increase between 140 and 100 m a.s.l. up to 72,000 #/cm^3, followed by a decrease down to 33,000 #/cm^3 at ground levels.

Simultaneously, particle growth was registered at ground until about 14:00, and a second relative increase in nitrate and organic aerosols was observed (Figs. 5 and 6). It is probable that the high $N_{>3}$

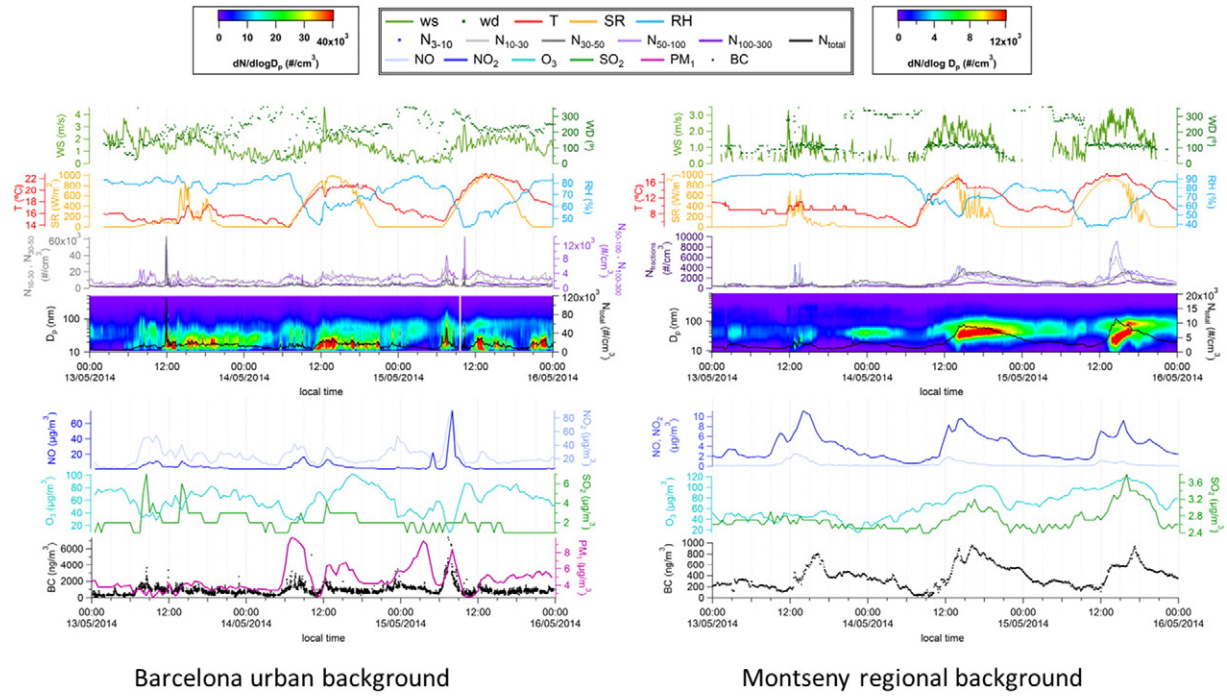

Fig. 5. Particle number size distribution, meteorological parameters, N, gaseous pollutants, PM_1 and black carbon (BC) measurements at the urban background site in Barcelona (left) and the regional background site at Montseny (right), from 13th to 15th May 2014.

recorded at different heights (much higher than the N concentrations at ground level) were caused by new particle formation episodes.

At Montseny regional background an average N_{15-100} of 3500 # cm^{-3} was recorded (Fig. 5). At 14:00 photochemical nucleation and subsequent particle growth also occurred as deduced from SMPS measurements, whose resulting particles merged with the pre-existing coarser regional background particles, increasing $N_{>3}$ levels up to 9500 # cm^{-3} (Fig. 5).

3.4. 15 May 2014 measurements

This was also a clear and warm day, with 17 to 25 °C and 37 to 64% RH at ground level, and from 12 to 18 °C and 44 to 64% RH at 850 m a.s.l. during the balloon measurements. The 5-day back trajectory indicates that the dominant air mass origin was from the Northwest, although the last day of the trajectory is only a few km long, which

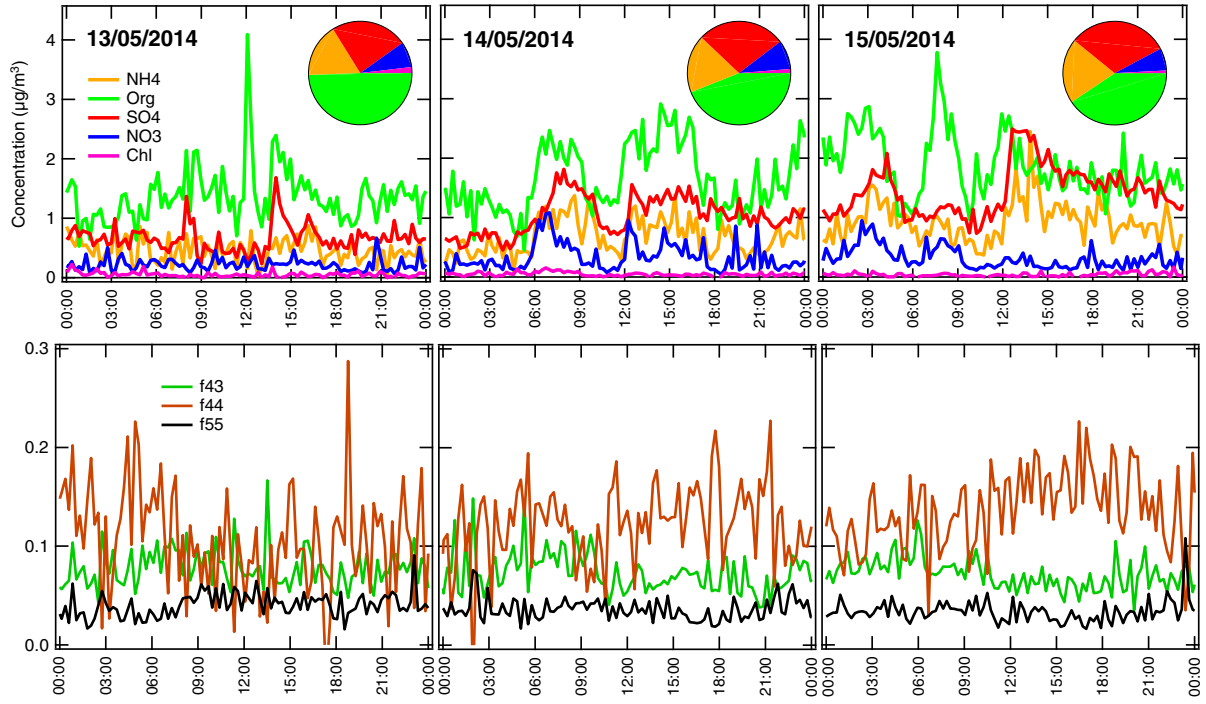

Fig. 6. Concentration of organics, sulfate, nitrate, ammonium and chloride measured with the ACSM at the urban background site in Barcelona during 13 to 15 May 2014. Time series of tracers of primary organic road traffic emissions (f55) and secondary organic compounds (f43 and f44).

indicates that the air masses on this day were the same as in the previous day (Fig. S2). The wind direction during the ascending flight turned from the W–NW at heights between 0 and 400–500 m a.s.l. to W–SW between 500 and 900 m a.s.l. (Fig. S3). According to the radiosoundings, the PBLH at 02:00 and 14:00 was around 700 and 1900 m a.s.l., respectively (Fig. 3). The vertical profile obtained from the tethered balloon in the early morning (08:00 to 09:30) indicated a lower PBLH of around 400 m a.s.l. (Fig. 3), which is in agreement with the change in wind direction recorded at 400–500 m a.s.l. This apparent discrepancy can be explained by the higher errors of the applied technique (the parcel method) in the absence of clear inversions, such as at the situation at 8:00 in the morning. It can also be due to the different times at which the PBLH was calculated, since the PBL may have not been developed at 8:00 but completely developed at 14:00.

The ascending flight (up to 900 m a.s.l.) took place during 8:00–9:30, coinciding with the traffic rush hour. During this time, particle size distributions at ground level reflect the influence of road traffic, with a maximum $N_{10–480}$ of 32,800 #/cm^3 and very high BC concentrations, reaching 6–7 μg/m^3 (Fig. 5). Simultaneously, increases in NO_2 (up to 70 μg/m^3), PM_1 (up to 8 μg/m^3), organic aerosols (reaching 3.5 μg/m^3) and $N_{20–100}$ (31,300 #/cm^3) were also recorded (Figs. 5 and 6). Balloon measurements (Figs. 4 and S4) show that $N_{>3}$ followed a clear upward decreasing trend from ground (52,000–66,000 #/cm^3) to around 240 m a.s.l. (6600 #/cm^3), followed by a transect from 240 to 530 m a.s.l. with constant intermediate levels (8500–19,500 #/cm^3) and a top section from 530 to 875 m a.s.l. with lower levels (5800–6700 #/cm^3), representing the free troposphere (Fig. 3). As described for the first flight on the 14 May, the bottom and intermediate sectors were characterized by an interlayering of strata with very different $N_{>3}$ (Fig. S4). The decrease of $N_{>3}$ with height in the lowest layer (ground-240 m a.s.l.) was associated with more stable conditions preventing the transport of UFP generated at ground level upwards. Concentrations of particles with size >0.3 μm evidenced a vertical profile where the same three transects described above can be identified, the two lower ones with clear upward decreasing trends (56 to 24 #/cm^3 and 24 to 8 #/cm^3 for the 0.3–0.5 μm particulate fraction) and the top one with an increasing trend (8 to 14 #/cm^3).

The descending flight took place only from 875 to 777 m a.s.l. (9:31 to 10:28), followed by measurements at around 777–644 m a.s.l. (altitude depending on the wind velocity) until 16:02. From 9:31 to 9:57 the $N_{>3}$ was typical from the free troposphere, 4600–7100 #/cm^3, but a progressive increase up to 78,500 #/cm^3 was recorded at 808–699 m a.s.l. from 9.57 to 11.35, probably due to the growth of the boundary layer reaching the measurement height (Fig. 7). The change in the RH and temperature recorded at 10:40 further indicates a change in the air mass (Fig. 7). These concentrations at this height are very high and they may be the result of new particle formation processes occurring as the ground emissions of precursors are diluted by the convective growth of the PBL under relatively low RH and high temperature and insolation. This is also supported by the constantly relatively low levels of BC recorded during this marked increase of $N_{>3}$ (Fig. 7). From 11:35 to 13:42 the $N_{>3}$ remained very high (45,300–96,600 #/cm^3), with the maximum being recorded at 13:38, very close to the maximum insolation time (14:00), and probably reflecting the occurrence of intense nucleation bursts (Fig. 7). During this time, very high UFP concentrations were also recorded at ground level and SMPS data show a new particle formation episode (Fig. 5), which indicates that new particle formation could have been taking place in the whole column over Barcelona. The arrival of relatively clean air masses with the sea breeze, maybe including SO_2 and other gaseous precursors, may also be responsible for the new particle formation taking place at the measuring site. High sulfate concentrations (about 2.5 μg/m^3) were recorded at ground level (Fig. 6), which may result from the new particle formation processes and subsequent growth of particles. Secondary organic aerosol also increased during this time, as shown by the high increase in *m/z* 44, which is not seen for the road traffic primary organic aerosol markers (Fig. 6). The $N_{10–480}$ at ground level remained high until approximately 13:30, coinciding with the maximum $N_{>3}$ recorded on height (Figs. 5 and 7). These high $N_{>3}$ were recorded with a range of RH from 44 to 71% and 14–19 °C at around 777–644 m a.s.l. Following this period, RH was kept at relatively higher values (57–72%) and temperature at lower ones (14–16 °C) and $N_{>3}$ progressively decreased down to 37,600 #/cm^3 at 14:00, and from then to the end of the measurements (16:02) levels ranged from 46,800 to 27,200 #/cm^3 (Fig. 7).

Levels of 0.3–0.5, 0.5–1.0 and 1.0–5.0 μm particulate fractions (Fig. 4) showed a similar trend to the one described for $N_{>3}$, with very low levels during early morning (12–16 #/cm^3 for the 0.3–0.5 μm particulate fraction) and a progressive increase until 11:49 (36–42 #/cm^3 for 0.3–0.5 μm) and relatively higher levels from then to the end of the measurements (42–71 #/cm^3) (Fig. 7). Hence, the coarser fractions seem to be less affected by insolation than UFP, but they depend more on the PBLH. Furthermore, relative peaks of their concentrations may be influenced by relative increases of wind velocity (Fig. 7), which cause convective flows transporting PM from ground level upwards. In any case, the maximum concentration of the >0.3 μm fraction is also influenced by the insolation, since it is recorded at 14:02 (Fig. 7). These high $N_{>3}$ and micronic particulate levels are typical from the boundary layer and not from the free troposphere, which is in agreement with the PBLH of around 1900 m a.s.l. determined by radiosounding measurements at 14:00.

At Montseny regional background site the pattern was similar to that described for the 14 May. There was a pool of particles in the sizes of 50–100 nm that persisted all day. The $N_{3–10}$ concentration was >3000 #/cm^3 from 14:00 to 16:00, reaching a peak of 9000 #/cm^3. At 14:00 the increase in particle number concentration may be attributed to an intensive new particle formation episode with subsequent growth, or to the arrival of previously formed particles transported to the sampling site (Fig. 5). In either case, a subsequent growth and eventual mixing with the pre-existent larger particles may have also occurred.

3.5. Microscopy analysis

TEM and SEM analysis of particles sampled at altitudes >600 m a.s.l. evidenced a high proportion of aged sea salt (Na–Mg–Cl–S–N rich particles), sulfate-bearing particles and mineral aggregates in the $PM_{1–2.5}$ and $PM_{2.5–10}$ fractions (Fig. S5). The $PM_{1–2.5}$ fraction was dominated by highly hygroscopic particles as deduced from the spherical shapes, probably originated by water condensation (Fig. S5a). These are made up in a large proportion by sea salt particles and ammonium sulfate (Fig. S5b and c). Furthermore, mineral (quartz, and aluminumsilicate particles, Fig. S5d and e) with irregular shapes were also present. In a minor proportion, the occurrence of soot particles (Fig. S5f and g), probably from vehicle exhaust emissions, and metallic fly ash (Fig. S5h) from industrial sources was also evidenced.

The semi-quantitative SEM-EDX analysis of $PM_{1–2.5}$ and $PM_{2.5–10}$ samples resulted in a ternary system of sulfate, sea salt, and mineral matter. The analysis revealed a relative increase of sea salt particles from ground to the top of the PBLH and to the free troposphere (16, 30, and 50% on the 14 May and 31, 44, and 66% for the 15 May). The opposite trend was found for mineral matter (from 70% to 39% on the 14 May, and from 46 to 14% on the 15 May) (Figs. S6 and S7). Finally, the relative abundance of sulfate particles is relatively homogenous, with a slight increase in the top of the PBLH.

4. Discussion and conclusions

The measurement campaign covered a period with different meteorological scenarios affecting new particle formation processes. Light rain took place on 12 May, which partly cleaned the atmosphere. The first day of measurements (13 May 2014) was cloudy with very light rain that prevented the development of intensive convective circulations due to the low insolation (Figs. 3 and 5). Low concentrations of BC, N, micronic PM and gaseous pollutants were recorded at ground level

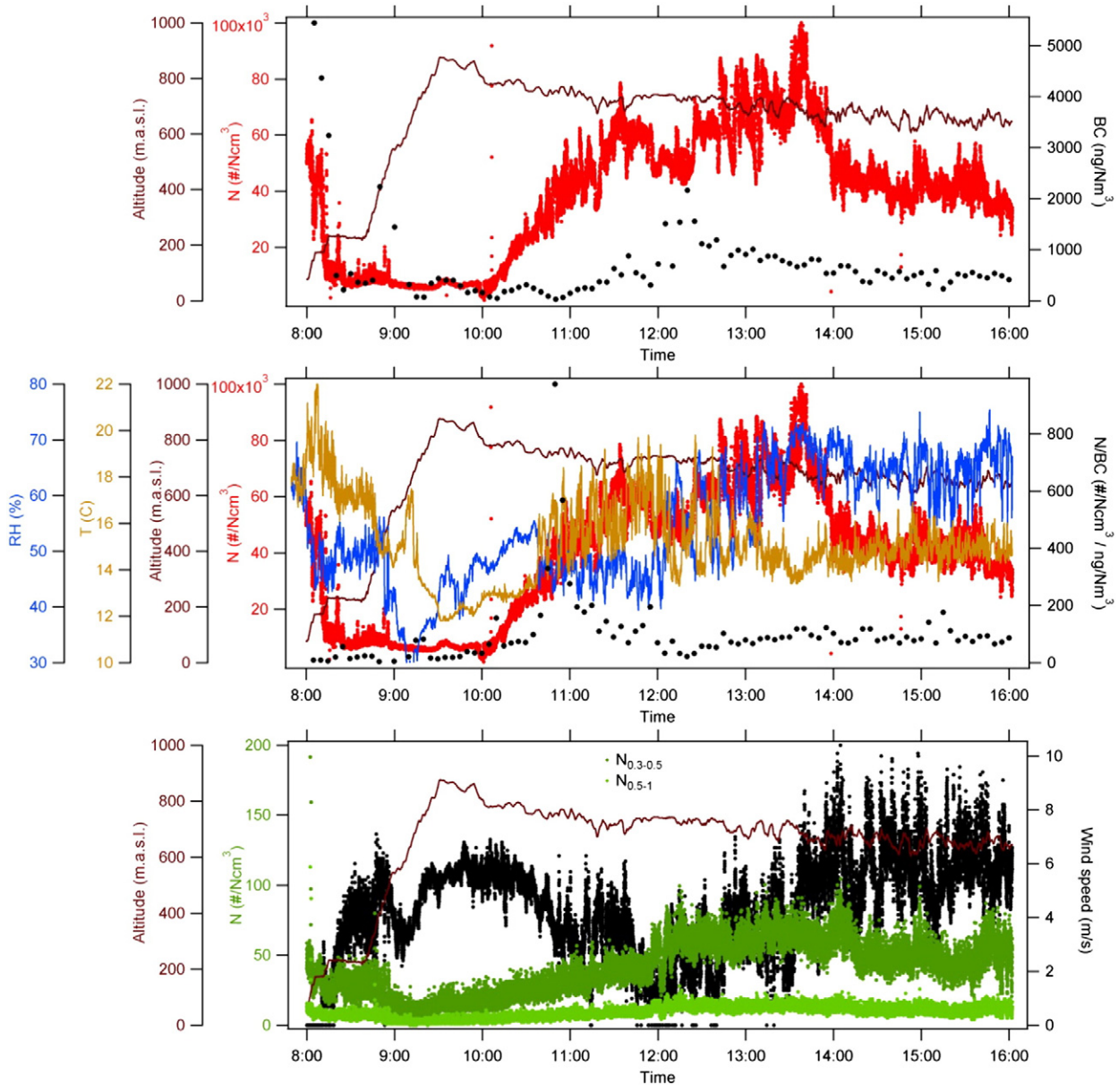

Fig. 7. Time evolution of $N_{>3}$, black carbon (BC), altitude, $N_{>3}$/BC ratio, relative humidity (RH), temperature (T), number concentration of particles from 0.3 to 0.5 μm and 0.5 to 1.0 μm ($N_{0.3-0.5}$, $N_{0.5-1.0}$) and wind speed of the ascending vertical profile and the subsequent constant height measurements carried out on 15 May 2014.

(both at the urban and the regional background sites, Figs. 5 and 6), as well as during the vertical measurements (Figs. 4 and S4). The low insolation also accounted for the absence of relevant new particle formation episodes over the city of Barcelona as ground pollution was being diluted.

During the second and third days (14 and 15 May 2014), meteorological conditions changed drastically leading to sunny clear-sky days. The very high insolation (Fig. 5) accounted for intense convective circulations that generated a very thick PBLH and injected and diluted ground pollutants to over 1000 m a.s.l. at midday (Fig. 3). High levels of traffic-related pollutants were measured during traffic rush hours at ground level (NO_2 > 90 μg/m^3, BC > 6 μg/m^3, Fig. 5; organic matter > 2 μg/m^3, nitrate > 0.5 μg/m^3, Fig. 6). The high insolation coupled to these high loads of pollutants, and probably regionally-emitted biogenic volatile organic compounds (VOCs), gave rise to high levels of O_3 (Fig. 5). This upwards urban thermal flow and dilution of pollutants in a very photochemically-favorable scenario probably caused continuous new particle formation episodes over the city, with a maximum reached at midday on the 15 May 2014, where $N_{>3}$ was above 90,000 #/cm^3 at around 800 m a.s.l. over the city (Figs. 4 and 7). Thus, the ratio $N_{>3}$/BC was close to 10 (#/cm^3/ng/m^3) at ground level during early morning, and it reached up to 50 at around 200 and 600 m a.s.l. Measurements done at a constant height (800–650 m a.s.l.) from early morning to the afternoon evidenced that the time evolution of $N_{>3}$ concentrations followed the insolation trend (Fig. 7), probably due to the photochemically driven new particle formation. In the period when the balloon (fixed at around 750 m a.s.l.) was reached by the boundary layer by the convective growth (from around 10:00 h to 11:30), as shown by the change in RH and temperature, the ratio $N_{>3}$/BC reached up to more than 800, one order of magnitude higher than during the rest of the measurements, and higher than the ratio at ground level, which was 20 at that time. This was probably caused by intensive new particle formation episodes in the top upper front of the boundary layer. The new particle formation may have remained active during the day given the $N_{>3}$/BC ratios between 50 and 120 registered at 750 m a.s.l. Particle concentration in the ranges of 0.3–0.5, 0.5–1.0 and 1.0–5.0 μm

followed also an increasing trend with time. The concentrations were relatively low in early morning, when the sampling point was above the PBLH, and reached higher values when the PBLH surpassed the sampling point height (750 m a.s.l.). However, once into the PBL, number concentration of particles >0.3 μm could be influenced by the wind speed (Fig. 7). This reflects probably the upward supply of ground particles >0.3 μm by convective circulations. TEM and SEM analysis of sampled particles at altitudes > 600 ma.s.l. evidenced a high proportion of aged sea salt, sulfate-bearing particles and mineral aggregates (Fig. S5) transported from the ground level.

The influence of the wind dynamics at a local scale on the UFP concentrations and coarser particles was investigated. No clear relation was observed between wind speed and $N_{>3}$. Nevertheless, an inverse relationship was found for the coarser particles (>0.3 μm), indicating particle advection processes when the balloon was kept at a constant height on the 15 May. After 12:00, however, the PBL grew over the balloon height and the particle concentration was mainly driven by local processes. Moreover, the standard deviation of the wind speed over given time intervals (2 min) was calculated as an indicator of turbulence. Whereas no relationship was found between turbulence and $N_{>3}$, a slight relationship with coarser particles was found, such that more intense turbulence leads to higher particle concentrations (Fig. S8). Hence, the behavior of the wind dynamics at very local scales does not have any influence on the production or removal of UFP, but it does on the coarser particles.

The ACSM ground measurements evidenced an increase in sulfate concentrations during the campaign, pointing to a progressive regional generation of sulfate. Moreover, the maximum sulfate load as well as the maximum concentration of secondary organic aerosol tracer *m/z* 44 were recorded around midday of the third day of measurements (15 May 2014), when maximum N concentrations were measured both at 800 m a.s.l. and at ground level (Figs. 5, 6 and 7). The occurrence of new particle formation processes during the second and third days was evidenced by the SMPS measurements at both regional and urban background sites (Fig. 5). Into the city, the duration of these new particle formation episodes at ground level was probably different than aloft: the high levels of pollution affecting the urban site during both morning and afternoon traffic rush hours increased the CS and prevented new particle formation; whereas at higher altitudes the upwards dilution may have allowed new particle formation during a longer period, as shown by the relatively high $N_{>3}$/BC ratios. Furthermore, when comparing the time of occurrence of new particle formation processes at the regional background site and at the urban site, new particle formation into the city started at around 11:00 at ground level on the 14 May 2014, whereas at the regional background site $N_{<20}$ increased only after 12:30 (Fig. 5). A similar situation was observed on the 15 May 2014, when new particle formation into the city was evident at 12:00, whereas at Montseny this occurred from 13:00 to 14:00 (Fig. 5), although it may have happened before near the sampling site with subsequent transport of particles. Thus, the fact that the new particle formation started before at the urban site than at the regional background in addition to the bigger size of particles in the regional background points to a probable urban origin of these episodes and not to a regional one, since a regional origin would lead to new particle formation starting at the same time at both sites, or even later at the urban site.

Fig. 8 shows an idealized and simplified model of the spatial and time occurrence of new particle formation episodes into, around (regional background) and over (at a given height) the city. Two types of scenario are described. For scenario 1, the new particle formation starts in the urban area and affects the regional background after particle growth while being transported away from the city. The scenario 1 corresponds to the two new particle formation episodes studied in our field campaign. The precursors are emitted in the city and urban photochemically-activated nucleation occurs both at ground and at high atmospheric levels (tens to hundreds of meters). At ground, new particle formation is limited by the high PM concentrations during

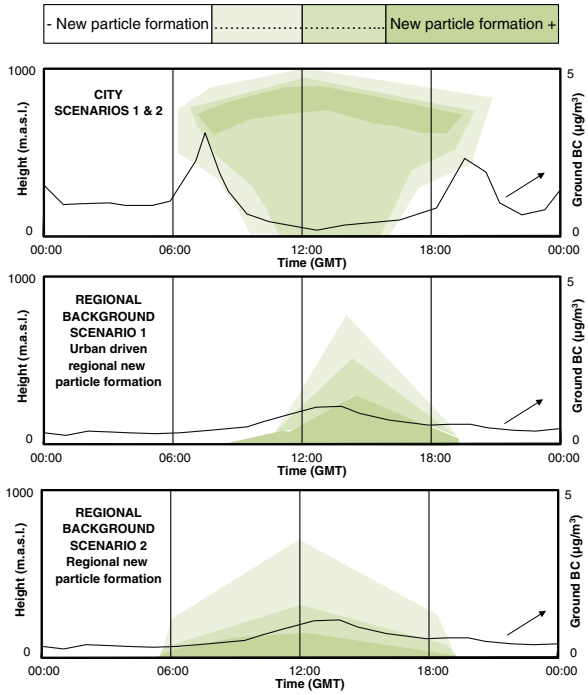

Fig. 8. Idealized model for the spatial and time occurrence of new particle formation episodes into, around (regional background) and over (at a given height) the city.

morning and evening traffic rush hours that increase the CS and prevent nucleation (Brines et al., 2014b) and hence it is restricted to midday and early afternoon. During this period pollution is diluted due to maximal sea breeze development and the relatively lower emissions, thus favoring new particle formation. A few hundred meters above the ground, levels of pollutants from the city are diluted and new particle formation may occur (as shown by the balloon measurements), even before midday as the thermally ascending polluted air mass is diluted. Thus, the highest $N_{>3}$ during the campaign was measured at midday at around 800 m a.s.l. above the city. The occurrence in the regional background is delayed, starting around midday when sea and mountain breezes transport the urban air mass towards the regional background site. At this time, a light increase of PM concentrations in the regional background is also observed as pollutants reach a relatively clean air mass (Fig. 8). This urban new particle formation, with delayed impact in the regional background site, was also observed by Dall'Osto et al. (2013) and Brines et al. (2014b), although only ground measurements were available for those studies.

The scenario 2 did not occur during the study period, but it has been described by Dall'Osto et al. (2013) and Brines et al. (2014b). It is characterized by the new particle formation having a regional origin. The new particle formation at the regional background site starts early in the morning and is probably driven both by photochemistry and an increase of precursors concentrations. Available SO_2 and biogenic VOCs emissions favor nucleation and substantially contribute to the growth of the ion clusters (Kulmala et al., 2004, 2013; Pierce, 2011). At the regional background the new particle formation and subsequent growth persists, during a long period, governed by insolation. The new particle formation pattern at ground level and over the city is similar to that described for scenario 1.

The scenario 1, corresponding to the one taking place during the measurements in the present study, agrees with the findings from Setyan et al. (2014), who showed that nucleation over foothills of Sierra Nevada area of California was enhanced when the plume of Sacramento affected the regional background area, and that the interaction between biogenic VOCs with urban plumes enhanced the nucleation and growth of particles. However, Cusack et al. (2013) and Dall'Osto et al. (2013)

found regional background new particle formation episodes that started early in the morning (09:00 GMT, not observed in the present study) before urban plumes reach the Montseny regional background site. These regional new particle formation episodes (scenario 2 in Fig. 8) probably occur around the Mediterranean basin due to the relatively high SO_2 background levels that shipping emissions cause in the region.

Although UFP concentrations are driven by road traffic emissions in most European urban areas, they can be highly influenced by new particle formation events in high insolation regions, taking place both at urban and at regional scales. This should be borne in mind when studying the impact of such particles in air quality, climate, and human health.

Acknowledgments

This study was partially funded by the European LIFE + AIRUSE project (LIFE11 ENV/ES/584), the Spanish Ministry of Agriculture, Food and the Environment (UCA2009020083), the Generalitat de Catalunya (AGAUR 2014 SGR33 and the DGQA) and the Korea Ministry of Environment through "The Eco-Innovation project". The authors acknowledge the Real Club de Polo de Barcelona for allowing the use of their facilities for the balloon flights and the Ajuntament de Barcelona.

Appendix A. Supplementary material

Supplementary data to this article can be found online at http://dx.doi.org/10.1016/j.atmosres.2015.05.003.

References

Ahn, K.H., Eun, H.R., 2013. Atmospheric aerosol measurement using tethered-balloon system and equipment development. 8th Asian Aerosol Conference, Sydney, Australia, 2–5 Dec 2013.

Alam, A., Shi, J.P., Harrison, R.M., 2003. Observations of new particle formation in urban air. J. Geophys. Res. 108 (D3), 4093. http://dx.doi.org/10.1029/2001JD001417.

Amato, F., Pandolfi, M., Escrig, A., Querol, X., Alastuey, A., Pey, J., Perez, N., Hopke, P.K., 2009. Quantifying road dust resuspension in urban environment by Multilinear Engine: a comparison with PMF2. Atmos. Environ. 43, 2770–2780.

Babu, S.S., Sreekanth, V., Moorthy, K.K., Mohan, M., Kirankumar, N.V.P., Subrahamanyam, D.B., Gogoi, M.M., Kompalli, S.K., Beegum, N., Chaubey, J.P., Kumar, V.H.A., Manchanda, R.K., 2011. Vertical profiles of aerosol black carbon in the atmospheric boundary layer over a tropical coastal station: perturbations during an annular solar eclipse. Atmos. Res. 99, 471–478.

Brines, M., Dall'Osto, M., Beddows, D.C.S., Harrison, R.M., Querol, X., 2014a. Simplifying aerosol size distributions modes simultaneously detected at four monitoring sites during SAPUSS. Atmos. Chem. Phys. 14, 2973–2986.

Brines, M., Dall'Osto, M., Beddows, D.C.S., Harrison, R.M., Gómez-Moreno, F., Núñez, L., Artíñano, B., Costabile, F., Gobbi, G.P., Salimi, F., Morawska, L., Sioutas, C., Querol, X., 2014b. Frequency of new particle formation events in the urban Mediterranean climate. Atmos. Chem. Phys. Discuss. 14, 26463–26494.

Canagaratna, M.R., Jayne, J.T., Ghertner, D.A., Herndon, S., Shi, Q., Jimenez, J.L., Silva, P.J., Williams, P., Lanni, T., Drewnick, F., Demerjian, K.L., Kolb, C.E., Worsnop, D.R., 2004. Chase studies of particulate emissions from in-use New York city vehicles. Aerosol Sci. Technol. 38, 555–573.

Charlson, R.J., Schwartz, S.E., Hales, J.M., Cess, R.D., Coakley Jr., J.A., Hansen, J.E., Hofmann, D.J., 1992. Climate forcing by anthropogenic aerosols. Science 255, 423–430.

Charron, A., Harrison, R.M., 2003. Primary particle formation from vehicle emissions during exhaust dilution in the roadside atmosphere. Atmos. Environ. 37, 4109–4119.

Cheung, H.C., Morawska, L., Ristovski, Z.D., 2011. Observation of new particle formation in subtropical urban environment. Atmos. Chem. Phys. 11, 3823–3833.

Cheung, H.C., Chou, C.C.-K., Jayaratne, E.R., Morawska, L., 2015. Impact of particle formation on atmospheric ions and particle number concentrations in an urban environment. Atmos. Res. 157, 127–136.

Costabile, F., Amoroso, A., Wang, F., 2010. Sub-μm particle size distributions in a suburban Mediterranean area. Aerosol populations and their possible relationship with HONO mixing ratios. Atmos. Environ. 44, 5258–5268.

Cusack, M., Alastuey, A., Querol, X., 2013. Case studies of new particle formation and evaporation processes in the western Mediterranean regional background. Atmos. Environ. 81, 651–659.

Dall'Osto, M., Thorpe, A., Beddows, D.C.S., Harrison, R.M., Barlow, J.F., Dunbar, T., Williams, P.I., Coe, H., 2011. Remarkable dynamics of nanoparticles in the urban atmosphere. Atmos. Chem. Phys. 11, 6623–6637.

Dall'Osto, M., Querol, X., Alastuey, A., O'Dowd, C., Harrison, R.M., Wenger, J., Gómez Moreno, F.J., 2013. On the spatial distribution and evolution of ultrafine particles in Barcelona. Atmos. Chem. Phys. 13, 741–759.

Draxler, R.R., Rolph, G.D., 2003. HYSPLIT (HYbrid Single-Particle Lagrangian Integrated Trajectory). NOAA Air Resources Laboratory, Silver Spring, MD (Model access via NOAA ARL READY Website (http://www.arl.noaa.gov/ready/hysplit4.html)).

Fernández-Gálvez, J., Guerrero-Rascado, J.L., Molero, F., Lyamani, H., Revuelta, M.A., Navas-Guzmán, F., Sastre, M., Bravo-Aranda, J.A., Fernández, A.J., Granados-Muñoz, M.J., Gómez-Moreno, F.J., Olmo, F.J., Pujadas, M., Alados-Arboledas, L., 2013. Aerosol size distribution from inversion of solar radiances and measured at ground-level during SPALI10 campaign. Atmos. Res. 127, 130–140.

Ferrero, L., Perrone, M.G., Petraccone, S., Sangiorgi, G., Ferrini, B.S., Lo Porto, C., Lazzati, Z., Cocchi, D., Bruno, F., Greco, F., Riccio, A., Bolzacchini, E., 2010. Vertically-resolved particle size distribution within and above the mixing layer over the Milan metropolitan area. Atmos. Chem. Phys. 10, 3915–3932.

Ferrero, L., Mocnik, G., Ferrini, B.S., Perrone, M.G., Sangiorgi, G., Bolzacchini, E., 2011. Vertical profiles of aerosol absorption coefficient from micro-Aethalometer data and Mie calculation over Milan. Sci. Total Environ. 409, 2824–2837.

Fujitani, Y., Kumar, P., Tamura, K., Fushimi, A., Hasegawa, S., Takahasi, K., Tanabe, K., Kobayashi, S., Hirano, S., 2012. Seasonal differences of the atmospheric particle size distribution in a metropolitan area in Japan. Sci. Total Environ. 437, 339–347.

Greenberg, J.P., Guenther, A.B., Turnipseed, A., 2009. Tethered balloon-based soundings of ozone, aerosols, and solar radiation near Mexico City during MIRAGE-MEX. Atmos. Environ. 43, 2672–2677.

Hara, K., Osada, K., Yamanouchi, T., 2013. Tethered balloon-borne aerosol measurements: seasonal and vertical variations of aerosol constituents over Syowa Station, Antarctica. Atmos. Chem. Phys. 13, 9119–9139.

Hara, K., Hayashi, M., Yabuki, M., Shiobara, M., Nishita-Hara, C., 2014. Simultaneous aerosol measurements of unusual aerosol enhancement in the troposphere over Syowa Station, Antarctica. Atmos. Chem. Phys. 14, 4169–4183.

Harris, S.J., Maricq, M.M., 2001. Signature size distributions for diesel and gasoline engine exhaust particulate matter. J. Aerosol Sci. 32, 749–764.

Harrison, R.M., Dall'Osto, M., Beddows, D.C.S., Thorpe, A.J., Bloss, W.J., Allan, J.D., Coe, H., Dorsey, J.R., Gallagher, M., Martin, C., Whitehead, J., Williams, P.I., Jones, R.L., Langridge, J.M., Benton, A.K., Ball, S.M., Langford, B., Hewitt, C.N., Davison, B., Martin, D., Petersson, K., Henshaw, S.J., White, I.R., Shallcross, D.E., Barlow, J.F., Dunbar, T., Davies, F., Nemitz, E., Phillips, G.J., Helfter, C., Di Marco, C.F., Smith, S., 2012. Atmospheric chemistry and physics in the atmosphere of a developed megacity (London): an overview of the REPARTEE experiment and its conclusions. Atmos. Chem. Phys. 12, 3065–3114.

Holzworth, G., 1967. Mixing depths, wind speeds and air pollution potential from selected locations in the United States. J. Appl. Meteorol. 6, 1039–1044.

Hudda, N., Cheung, K., Moore, K.F., Sioutas, C., 2010. Inter-community variability in total particle number concentrations in the easter Los Angeles air basin. Atmos. Chem. Phys. 10, 11385–11399.

IPCC, 2013. Assessment Report of the Intergovernmental Panel on Climate Change. Cambridge Univ. Press, Cambridge, UK (available at: https://www.ipcc.ch/report/ar5/wg1/ (last access: June 2014)).

Kittelson, D.B., Watts, W.F., Johnson, J.P., 2004. Nanoparticle emissions on Minnesota highways. Atmos. Environ. 38, 9–19.

Kulmala, M., Kerminen, V.M., 2008. On the formation and growth of atmospheric nanoparticles. Atmos. Res. 90, 132–150.

Kulmala, M., Vehkamäki, H., Petaäjä, T., Dal Maso, M., Lauri, A., Kerminen, V.-M., Birmili, W., McMurry, P.H., 2004. Formation and growth rates of ultrafine atmospheric particles: a review of observations. J. Aerosol Sci. 35, 143–176.

Kulmala, M., Kontkanen, J., Junninen, H., Lehtipalo, K., Manninen, H.E., Nieminen, T., Petäjä, T., Sipilä, M., Schobesberger, S., Rantala, P., Franchin, A., Jokinen, T., Järvinen, E., Äijälä, M., Kangasluoma, J., Hakala, J., Aalto, P.P., Paasonen, P., Mikkilä, J., Vanhanen, J., Aalto, J., Hakola, H., Makkonen, U., Ruuskanen, T., Mauldin, R.L., Duplissy, J., Vehkamäki, H., Bäck, J., Kortelainen, A., Riipinen, I., Kurtén, T., Johnston, M.V., Smith, J.N., Ehn, M., Mentel, T.F., Lehtinen, K.E.J., Laaksonen, A., Kerminen, V.-M., Worsnop, D.R., 2013. Direct observations of atmospheric aerosol nucleation. Science 339, 943–946.

Kumar, P., Morawska, L., Birmili, W., Paasonen, P., Hu, M., Kulmala, M., Harrison, R.M., Norford, L., Britter, R., 2014. Ultrafine particles in cities. Environ. Int. 66, 1–10.

Lee, H.-K., Hwang, I.-K., Ahn, K.-H., 2014. Development and evaluation of Hy-CPC, Particle and Aerosol Research 10, 3 93–97 http://dx.doi.org/10.11629/jpaar.2014.10.3.093.

Ma, X., Yu, F., 2014. Seasonal variability of aerosol vertical profiles over east US and west Europe: GEOS-Chem/APM simulation and comparison with CALIPSO observations. Atmos. Res. 140–141, 28–37.

Makkonen, R., Asmi, A., Kerminen, V.-M., Boy, M., Arneth, A., Hari, P., Kulmala, M., 2012. Air pollution control and decreasing new particle formation lead to strong climate warming. Atmos. Chem. Phys. 12, 1515–1524.

Matsuki, A., Iwasaka, Y., Shi, G.-Y., Chen, H.-B., Osada, K., Zhang, D., Kido, M., Inomata, Y., Kim, Y.-S., Trochkine, D., Nishita, C., Yamada, M., Nagatani, T., Nagatani, M., Nakata, H., 2005. Heterogeneous sulfate formation on dust surface and its dependence on mineralogy: Balloon-borne observations from balloon-borne measurements in the surface atmosphere of Beijing, China. Water Air Soil Pollut. Focus 5, 101–132.

Millán, M., Mantilla, E., Salvador, S., Carratalá, A., Sanz, M.J., Alonso, L., Gangoti, G., Navazo, M., 2000. Ozone cycles in the Western Mediterranean Basin: interpretation of monitoring data in complex coastal terrain. J. Appl. Meteorol. 39, 487–508.

Morawska, L., Thomas, S., Bofinger, N., Wainwright, D., Neale, D., 1998. Comprehensive characterization of aerosols in a subtropical urban atmosphere: particle size distribution and correlation with gaseous pollutants. Atmos. Environ. 32, 2467–2478.

Moroni, B., Cappelletti, D., Marmottini, F., Scardazza, F., Ferrero, L., Bolzacchini, E., 2012. Integrated single particle-bulk chemical approach for the characterization of local and long range sources of particulate pollutants. Atmos. Environ. 50, 267–277.

Moroni, B., Ferrero, L., Crocchianti, S., Perrone, M.G., Sangiorgi, G., Bolzacchini, E., Cappelletti, D., 2013. Aerosol dynamics upon Terni basin (Central Italy): results of

integrated vertical profile measurements and electron microscopy analyses. Rend. Lincei 24, 319–328.
Ng, N.L., Herndon, S.C., Trimborn, A., Canagaratna, M.R., Croteau, P.L., Onasch, T.B., Sueper, D., Worsnop, D.R., Zhang, Q., Sun, Y.L., Jayne, J.T., 2011. An Aerosol Chemical Speciation Monitor (ACSM) for routine monitoring of the composition and mass concentrations of ambient aerosol. Aerosol Sci. Technol. 45, 770–784.
Padró-Martínez, L.T., Patton, A.P., Trull, J.B., Zamore, W., Brugge, D., Durant, J.L., 2012. Mobile monitoring of particle number concentration and other traffic-related air pollutants in a near-highway neighbourhood over the course of a year. Atmos. Environ. 61, 253–264.
Pandolfi, M., Querol, X., Alastuey, A., Jimenez, J.L., Jorba, O., Day, D., Ortega, A., Cubison, M.J., Comerón, A., Sicard, M., Mohr, C., Prévôt, A.S.H., Minguillón, M.C., Pey, J., Baldasano, J.M., Burkhart, J.F., Seco, R., Peñuelas, J., van Drooge, B.L., Artiñano, B., Di Marco, C., Nemitz, E., Schallhart, S., Metzger, A., Hansel, A., Lorente, J., Ng, S., Jayne, J., Szidat, S., 2014. Effects of sources and meteorology on particulate matter in the Western Mediterranean Basin: an overview of the DAURE campaign. J. Geophys. Res. Atmos. 119. http://dx.doi.org/10.1002/2013JD021079.
Pérez, C., Sicard, M., Jorba, O., Comerón, A., Baldasano, J.M., 2004. Summertime re-circulations of air pollutants over the northeastern Iberian coast observed from systematic EARLINET lidar measurements in Barcelona. Atmos. Environ. 38, 3983–4000.
Pérez, N., Pey, J., Castillo, S., Viana, M., Alastuey, A., Querol, X., 2008. Interpretation and variability of levels of regional background aerosols in the Western Mediterranean. Sci. Total Environ. 1, 527–540.
Pérez, N., Pey, J., Cusack, M., Reche, C., Querol, X., Alastuey, A., Viana, M., 2010. Variability of particle number, black carbon, and PM10, PM2.5, and PM1 levels and speciation: influence of road traffic emissions on urban air quality. Aerosol Sci. Technol. 44, 487–499.
Petzold, A., Ogren, J.A., Fiebig, M., Laj, P., Li, S.-M., Baltensperger, U., Holzer Popp, T., Kinne, G., Pappalardo, G., Sugimoto, N., Wehrli, C., Wiedensohler, A., Zhang, X.-Y., 2013. Recommendations for reporting "black carbon" measurements. Atmos. Chem. Phys. 13, 8365–8379.
Pey, J., Rodríguez, S., Querol, X., Alastuey, A., Moreno, T., Putaud, J.P., Van Dingenen, R., 2008. Variations of urban aerosols in the western Mediterranean. Atmos. Environ. 42, 9052–9062.
Pey, J., Querol, X., Alastuey, A., Rodríguez, S., Putaud, J.P., Van Dingenen, R., 2009. Source apportionment of urban fine and ultrafine particle number concentration in a Western Mediterranean city. Atmos. Environ. 43, 4407–4415.
Pierce, J., 2011. Atmospheric chemistry: particulars of particle formation. Nat. Geosci. 4, 665–666.
Reche, C., Querol, X., Alastuey, A., Viana, M., Pey, J., Moreno, T., Rodríguez, S., González, Y., Fernández-Camacho, R., de la Rosa, J., Dall'Osto, M., Prévôt, A.S.H., Hueglin, C., Harrison, R.M., Quincey, P., 2011. New considerations for PM, Black Carbon and particle number concentration for air quality monitoring across different European cities. Atmos. Chem. Phys. 11, 6207–6227.
Robinson, A.L., Donahue, N.M., Shrivastava, M.K., Weitkamp, E.A., Sage, A.M., Grieshop, A.P., Lane, T.E., Pierce, J.R., Pandis, S.N., 2007. Rethinking organic aerosols: semivolatile emissions and photochemical aging. Science 315, 1259.
Rodríguez, S., Van Dingenen, R., Putuad, J.-P., Dell'Acqua, A., Pey, J., Querol, X., Alastuey, A., Chenery, S., Ho, K.-F., Harrison, R., Tardivo, R., Scarnato, B., Gemelli, V., 2007. A study on the relationship between mass concentrations, chemistry and number size distribution of urban fine aerosols in Milan, Barcelona and London. Atmos. Chem. Phys. 35, 217–232.
Rose, D., Wehner, B., Ketzel, M., Engler, C., Voigtländer, J., Tuch, T., Wiedensohler, A., 2006. Atmospheric number size distributions of soot particles and estimation of emission factors. Atmos. Chem. Phys. 6, 1021–1031.
Salma, I., Borsos, T., Nemeth, Z., Weidiger, T., Aalto, P., Kulmala, M., 2014. Comparative study of ultrafine atmospheric aerosol within a city. Atmos. Environ. 92, 154–161.
Seco, R., Peñuelas, J., Filella, I., Llusià, J., Molowny-Horas, R., Schallhart, S., Metzger, A., Müller, M., Hansel, A., 2011. Contrasting winter and summer VOC mixing ratios at a forest site in the Western Mediterranean Basin: the effect of local biogenic emissions. Atmos. Chem. Phys. 11, 20389–20431.
Setyan, A., Song, C., Merkel, M., Knighton, W.B., Onasch, T.B., Canagaratna, M.R., Worsnop, D.R., Wiedensohler, A., Shilling, J.E., Zhang, Q., 2014. Chemistry of new particle growth in mixed urban and biogenic emissions—insights from CARES. Atmos. Chem. Phys. 14, 6477–6494.
Spracklen, D.V., Carslaw, K.S., Merikanto, J., Mann, G.W., Reddington, C.L., Pickering, S., Ogren, J.A., Andrews, E., Baltensperger, U., Weingartner, E., Boy, M., Kulmala, M., Laakso, L., Lihavainen, H., Kivekäs, N., Komppula, M., Mihalopoulos, N., Kouvarakis, G., Jennings, S.G., O'Dowd, C., Birmili, W., Wiedensohler, A., Weller, R., Gras, J., Laj, P., Sellegri, K., Bonn, B., Krejci, R., Laaksonen, A., Hamed, A., Minikin, A., Harrison, R.M., Talbot, R., Sun, J., 2010. Explaining global surface aerosol number concentrations in terms of primary emissions and particle formation. Atmos. Chem. Phys. 10, 4775–4793.
Stanier, C.O., Khlystov, A.Y., Pandis, S.N., 2004. Nucleation events during the Pittsburgh air quality study: description and relation to key meteorological, gas phase, and aerosol parameters. Aerosol Sci. Technol. 38 (S1), 253–264.
Vaisala, O., 2013. Humidity Conversion Formulas, published by Vaisala, Helsinki. http://www.vaisala.com/Vaisala%20Documents/Application%20notes/Humidity_Conversion_Formulas_B210973EN-F.pdf.
von Bismarck-Osten, C., Birmili, W., Ketzel, M., Massling, A., Petäjä, T., Weber, S., 2013. Characterization of parameters influencing the spatio-temporal variability of urban particle number size distributions in four European cities. Atmos. Environ. 77, 415–429.
Wehner, B., Birmili, W., Gnauk, T., Wiedensohler, 2002. Particle number size distributions in a street canyon and their transformation into the urban-air background. Atmos. Environ. 36, 2215–2223.
Wehner, B., Siebert, H., Stratmann, F., Tuch, T., Wiedensohler, A., Petäjä, T., Dal Maso, M., Kulmala, M., 2007. Horizontal homogeneity and vertical extent of new particle formation events. Tellus Ser. B 59, 362–371.
Wiedensohler, A., Birmili, W., Nowak, A., Sonntag, A., Weinhold, K., Merkel, M., Wehner, B., Tuch, T., Pfeifer, S., Fiebig, M., Fjäraa, A.M., Asmi, E., Sellegri, K., Depuy, R., Venzac, H., Villani, P., Laj, P., Aalto, P., Ogren, J.A., Swietlicki, E., Williams, P., Roldin, P., Quincey, P., Hüglin, C., Fierz-Schmidhauser, R., Gysel, M., Weingartner, E., Riccobono, F., Santos, S., Grüning, C., Faloon, K., Beddows, D., Harrison, R., Monahan, C., Jennings, S.G., O'Dowd, C.D., Marinoni, A., Horn, H.-G., Keck, L., Jiang, J., Scheckman, J., McMurry, P.H., Deng, Z., Zhao, C.S., Moerman, M., Henzing, B., de Leeuw, G., Löschau, G., Bastian, S., 2012. Mobility particle size spectrometers: harmonization of technical standards and data structure to facilitate high quality long-term observations of atmospheric particle number size distributions. Atmos. Meas. Tech. 5, 657–685.
Woo, K.S., Chen, D.R., Pui, D.Y.H., McMurry, P.H., 2001. Measurement of Atlanta aerosol size distributions: observations of ultrafine particle events. Aerosol Sci. Technol. 34, 75–87.
Zhang, Q., Alfarra, M.R., Worsnop, D.R., Allan, J.D., Coe, H., Canagaratna, M.R., Jimenez, J.L., 2005. Deconvolution and quantification of hydrocarbon-like and oxygenated organic aerosols based on aerosol mass spectrometry. Environ. Sci. Technol. 39, 4938–4952.
Zhu, Y., Hinds, W.C., Kim, S., Shen, S., Sioutas, C., 2002. Study of ultrafine particles near a major highway with heavy-duty diesel traffic. Atmos. Environ. 36, 4323–4335.